energies

MDPI

*Article*

# Identification of the Technical Condition of Induction Motor Groups by the Total Energy Flow

**N. I. Koteleva *, N. A. Korolev and Y. L. Zhukovskiy**

Educational Research Center for Digital Technologies, Saint Petersburg Mining University, 191106 Saint Petersburg, Russia; korolev_na@pers.spmi.ru (N.A.K.); zhukovskiy_yul@pers.spmi.ru (Y.L.Z.)
* Correspondence: Koteleva_NI@pers.spmi.ru; Tel.: +795-2377-1801

**Abstract:** The paper discusses the method of identifying the technical condition of induction motors by classifying the energy data coming from the main common power bus. The work shows the simulation results of induction motor operation. The correlation between occurring defects and current diagrams is presented. The developed simulation model is demonstrated. The general algorithm for conducting experiments is described. Five different experiments to develop an algorithm for the classification are conducted: determination of the motors number in operation with different power; determination of the motors number in operation with equal power; determination of the mode and load of induction electric motor; determination of the fault and its magnitude with regard to operation and load of induction motor; determination of the fault and its magnitude with regard to operation and load of induction motor with regard to non-linear load in the flow. The article also presents an algorithm for preprocessing data to solve the classification problem. In addition, the classification results are shown and recommendations for testing and using the classification algorithm on a real object are made.

**Keywords:** classification algorithm; induction electric motor; simulation model; the coefficient of electromagnetic momentum ripple; current harmonic distortion factor



**Citation:** Koteleva, N.I.; Korolev, N.A.; Zhukovskiy, Y.L. Identification of the Technical Condition of Induction Motor Groups by the Total Energy Flow. *Energies* **2021**, *14*, 6677. https://doi.org/10.3390/en14206677

Received: 12 August 2021
Accepted: 9 October 2021
Published: 14 October 2021



## 1. Introduction

One of the significant trends resulting from the growing technological, environmental, economic and social challenges to the fuel, energy and mineral complex is the transition to industry 4.0 production enterprises [1]. Digital transformation, or digitalization, is taking place, based on a redesign of business forms focused on the digital representation of data [2].

Electromechanical systems are widely used for general industrial applications, industrial plants, power generation facilities and mineral resource enterprises [3,4]. The electric motor is a key link in the emergence of robotic production and autonomous factories, as well as in the development of remote areas [5]. Therefore, a state assessment of currently used electrical equipment, timely diagnostics of emergency and pre-emergency modes of its operation and evaluation of remaining resources are of particular importance [6]. Despite the fact that an enterprise within the framework of digital transformation strives to switch to state forecasting of its assets, the complexity and high cost of applying damage detection and control systems for each piece of equipment are not conducive to enterprises changing the existing system of regulated repair [7]. This system involves a transition from electrical equipment to components with new products at fixed intervals. However, this approach does not take into account the actual load of the equipment and its current technical condition. Thus, downtime and even replacement of equipment that has not yet exhausted its service life are possible. At the same time there is a possibility of sudden failures if the equipment exhausts its resource earlier than planned. In this case, the economic effect of repair work is often unreasonably low.

Repair and maintenance costs of electrical equipment account for a significant part of the total operating costs of enterprises, especially within the mining industry [8]. Moreover, their total share in the process of operation increases. The complexity of electrical equipment technical diagnostics within technological complexes in the mining, oil and gas industry is caused by its broad nomenclature, specificity of execution and operating modes, as well as complex operating conditions and location in hard-to-reach places which are dangerous in terms of personnel presence [9].

The purpose of diagnostics of electric machine units is to increase their reliability and their technical service life. Greater reliability is achieved through early detection of defects and malfunctions, which allows them to be eliminated during maintenance, and in turn will exclude failures during operation [10].

Malfunctions of individual machine components that are not detected in time can lead to severe production accidents as well as unplanned downtime, lost profits and environmental damage [11]. The transition from maintenance according to regulations or equipment failure to maintenance according to the actual state, and subsequently to proactive maintenance based on prediction and modeling, requires the use of a comprehensive diagnostic method. This approach helps to detect defects. With a given probability, it predicts the duration of the state serviceability without the withdrawal of equipment for repair.

Methods and technical means of non-destructive testing of industrial electrical equipment are constantly developing [12,13]. The application of neural networks in equipment condition diagnostic tasks is not novel [14,15]. A number of papers discussing different ways to apply neural networks to equipment diagnostics are shown further in the text.

The following works (Janssens O. et al.) [16] and (Jing L. et al.) [17] discuss convolutional neural networks, which are used for diagnostics of electromechanical equipment condition. The basic idea is to automate the selection of significant features that affect the diagnosis. In contrast to the classical methods, where the features are classified manually, the proposed method gives higher accuracy and speed of results.

The paper (Han T. et al.) [18] presents an approach that improves the results of neural networks in diagnosing the equipment condition. The deep adversarial convolutional neural network (DACNN) is proposed as an improvement of the convolutional neural network. DACNN adds an additional discriminant classifier and introduces adversarial learning.

The article (Szymahski Z. et al.) [19] considers a specialized expert system "Diagnoprzem" and "HELMOS" (computer knowledge based expert system (KBES)) [20,21] for diagnosing faults in generators and distribution substations. The diagnostic system is designed for mining lifting and transport equipment. A detailed description and the results of industrial tests of this system are given.

The paper (Rizzoni G. et al.) [22] examines an overview of the parameters required for vehicle diagnostics. It shows the requirements for on-board diagnostics, the main problems associated with meeting these requirements, and describes the prospects for future research in this area.

The work (Barbieri G. et al.) [23] shows the development of condition-based predictive maintenance (CBPdM) in an Industry 4.0 environment. A case study for training in fault diagnosis approach (FDA) using a problem-based learning (PBL) approach is proposed.

This article (Hernandez J. D. et al.) [24] proposes a human-computer-machine interaction (HCMI) diagnostic system architecture. The proposed architecture approximates the requirements of Industry 4.0 and enables real-time diagnostics and maintenance by the operator.

The study (Wu F. et al.) [25] offers an interactive adaptive maintenance method for mechanical systems based on timely fault detection. For the timely detection of faults, the paper proposes using neural networks (self-organizing map (SOM) method), which allows the local clusters for patterns to be reduced, therefore reducing the computational load.

The paper (Chao M. A. et al.) [26] presents evidence for the effectiveness of deep learning in fault diagnosis. The work considers the data of advanced gas turbine condition monitoring under in-flight conditions with simulation of one serviceable and four faulty cases in the dynamic commercial modular aero-propulsion system simulation (C-MAPSS).

Wind turbine fault detection using highly imbalanced real SCADA data [27] describes the methodology of fault detection. It is based on the data analysis coming from the SCADA system applying neural network algorithms.

Having studied the mentioned works, it can be concluded that the use of various neural network algorithms to diagnose the condition of equipment is relevant.

The main hypothesis of the present article is that the state of induction motors connected to the common power supply bus can be identified using the electrical components (current and voltage). These are recorded on the common section bus by classifying and recognizing a particular motor condition during normal operation and when a defect occurs.

The major idea of the method proposed in the paper is to determine the defects of electric motors connected to a single power supply bus according to the energy characteristics taken on a common bus. That is, the diagnosis of equipment condition is carried out based on the analysis of common data for all induction motors. The proposed solution is considered to simplify the task of diagnosis and solve a number of disadvantages arising from the individual diagnosis. Such disadvantages include: the need to increase the number of primary transducers (current and voltage sensors) for individual recording of energy characteristics for each machine, reducing system reliability (due to the required calibration and the state of the sensors themselves), the need for a multi-channel ADC, etc. However, the implementation of this method requires a significant complication of the mathematical apparatus used to diagnose the equipment. As such a mathematical apparatus, it is recommended to use a classifier based on the principles of machine learning in the course of the work.

## 2. Materials and Methods

Figure 1 shows a simplified scheme of power supply with a visualization of the basic idea of operation. The scheme has a reference voltage waveform and corresponds to the quality of electrical energy.

As shown in Figure 1, the compensated type Hall-effect current sensors and the energy parameter control sensors on the individual power supply line of each motor are removed, and the energy parameter control sensors on the general power flow are installed. The results of statistical analysis searching for the causes of induction motor [28,29] failures show that the main types of defects, considered as bearing wear, air gap eccentricity, turn-to-turn faults and breakage of rotor rods are described by harmonic components of current [30,31]. It should be noted that turn-to-turn short circuits are the most challenging due to the high rate of development and consequences (1):

$$i_d(t) = I_{d.st}\sin\left(\omega_1\left[\frac{n}{p}(1-s)\pm k\right]t\right) = \sum_{di=1}^{di=\infty} I_{di}\sin(\omega_{di1}t), \quad (1)$$

where:

$I_{d.st}$—amplitude values of stator currents modulated at turn-to-turn faults;
$\omega_1$ = $2\pi f_1$—rotor speed (rad/s), $f_1$ = 50 Hz;
$s$—induction motor slip;
$n$ = 1,5,7...—the multiplicity of the main $\omega_1$ speed;
$k$ = 1,3 ... —odd integer;
$p$—number of pole pairs.

Taking into account (1), the stator current $I_{st}$ in the presence of faults in an induction motor is determined by the expression (2).

$$I_{st}(t) = I_1\sin(n\omega_1 t+\varphi) + \sum_{di=1}^{di=\infty} I_{di}\sin(\omega_{di1}t+\varphi) \quad (2)$$

where:

$I_1$—stator current amplitude values (A), power system;

$I_{di}$—stator current amplitude values (A), corresponding to the defect;

$\omega_{di} = 2\pi f_{di}$—rotation frequency of the harmonic component of the stator current caused by the defect (rad/s);

$f_{di}$—frequency defect (Hz);

$\varphi$—shift angle between fundamental harmonic of phase current and voltage (rad).

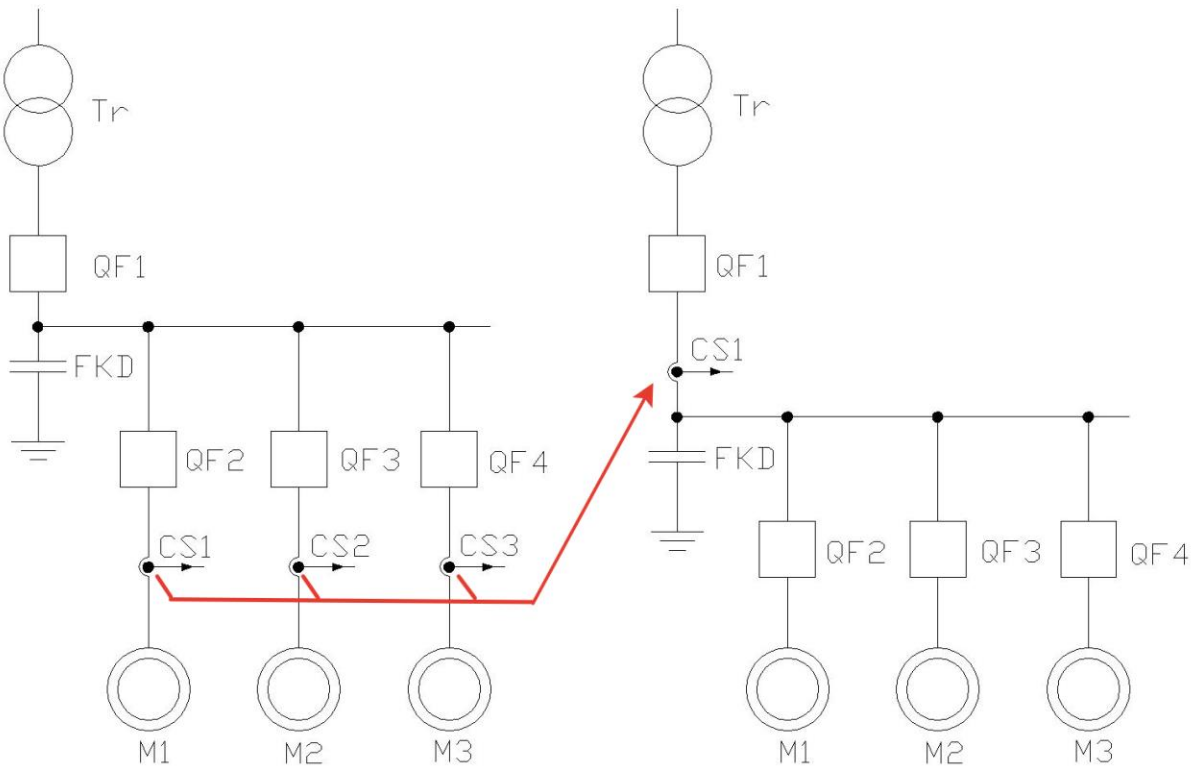


**Figure 1.** Simplified power supply systems. *left—with individual motor control; right—with control by total energy flow; Tr—transformer; QF—circuit breaker; FKD—filter-compensating devices; CS—Hall-effect current sensors compensated type; M—induction motors*.

In this case, the current harmonic distortion factor, taking in consideration Formulas (1) and (2), is presented as two components (3).

$$K_I = \frac{\sqrt{\left(K_{I(A)} + K_{I*(A)}\right)^2 + \left(K_{I(B)} + K_{I*(B)}\right)^2 + \left(K_{I(C)} + K_{I*(C)}\right)^2}}{3}, \quad (3)$$

where:

$K_{I(n)}$—current harmonic distortion factor, determined by the quality of electrical energy of the supply network in phases A, B, C;

$K_{I*}$—current harmonic distortion factor in phases A, B, C of the electric motor, determined by defects.

Distortions in the stator current lead to non-sinusoidal current and a decrease in the power factor, as well as being the torque-forming value of the electromagnetic torque $M_e$ of an induction motor (4).

$$M_e = \frac{3}{2} z_p \cdot \frac{L_m}{L_r} \cdot I_{st} \cdot \psi_r \cdot \sin(\theta), \quad (4)$$

where:

$z_p$—number of pole pairs of induction motor;

$L_m$—magnetization inductance;

$L_r$—rotor winding inductance;

$\psi_r$—rotor flux linkage;

$\theta$—angle between stator current vectors $I_{st}$ and rotor flux linkage $\psi_r$.

Thus, constant electromagnetic moment is formed by the interaction of harmonics of stator current and rotor flux linkage of the same order, multiple of fundamental frequency. Interaction of harmonics of different orders leads to the formation of pulsating components of electromagnetic moment. Pulsating electromagnetic moments can be divided into components determined by defects in the electrical or mechanical parts of the induction motor. So, the resulting electromagnetic moment can be represented as (5).

$$M_e = M_{(n)} + M_{(di)} = \sum_{n=1}^{n=\infty} I_{st} \cdot \psi_r \cdot \sin(\theta) + \sum_{i=1}^{i=\infty} I_{st(di)} \cdot \psi_{r(di)} \cdot \sin(\theta_{di}), \quad (5)$$

where:

$M_{(n)}$, $M_{(di)}$—components of electromagnetic moment (Nm) resulting from the interaction of n-th harmonics of stator current and rotor flux linkage, *di*-th harmonics of stator current and rotor flux linkage;

$I_{st(n)}$, $I_{st(di)}$, $\psi_{r(n)}$, $\psi_{r(di)}$—harmonic components of stator current and rotor flux linkage (A, Wb);

$\theta_{(di)}$—angle between di-th harmonics of stator current and rotor flux linkage (rad).

The coefficient of electromagnetic momentum ripple, determined as (6), is divided into components considering (4), (5) in the form of (7).

$$K_p = \frac{\sqrt{\sum_{n=2}^{n=\infty} M_{(n)}^2}}{M_{av}}, \quad (6)$$

$$\sum K_p = \frac{\sqrt{\sum_{n=2}^{n=\infty} M_{(n)}^2}}{M_{av}} + \frac{\sqrt{\sum_{i=2}^{i=\infty} M_{(di)}^2}}{M_{av}} = K_{p(n)} + K_p^*, \quad (7)$$

where:

$M_{av}$—average value of electromagnetic moment of induction motor (Nm);

$K_{p(n)}$—the coefficient of electromagnetic moment ripple, determined by the quality of the supply network and the design features of the electric motor;

$K_p^*$—the coefficient of electromagnetic moment ripple, determined by the type and level of motor and mechanical part of the electric motor defect.

Simulating the state of the induction electric motor and its defects, based on Formulas (1)–(7), we can see the changes in its energy characteristics when defects occur. This task is the first in the present work and is solved in order to obtain evidence of the correlation between the state of electric motors and their energy parameters.

An important stage of classification is the data preparation stage [32,33]. The main purpose is to identify the essential features. At the data preparation step for classification there is an allocation of essential features of the data sample. In terms of the induction electric motor state classification system, the use of data arrays (current values by phases and voltages) obtained at a certain moment of time are obvious. Thus, the input of the algorithm performing the classification is an array of values of dimensions 4 × 1, where the matrix rows contain the values of $I_A$, $I_B$ and $I_C$ and time t, at which these values are obtained. However, when we consider the theory of data processing and the theory of electric drive, we can see that this method does not allow the allocation of a significant number of features for defect classification. Not only the current, but also the previous values over a period of time, usually comparable to the frequency in electrical networks, are important in determining the defects. In Russia, it is 0.2 s. For example, in [34] it is proposed to divide the measured data received from the motor into frames. We can take the period of oscillation of a sinusoid as the length of such a frame. Since the frequency is stable and equal to 50 Hz, the period is also unchanged and equal to 0.02 s. At a frequency of 0.1 ms, a matrix of considerable size should be used as the input data, which negatively affects the quality and speed of classification. The preprocessing algorithm proposed in this work is shown in Figure 2.

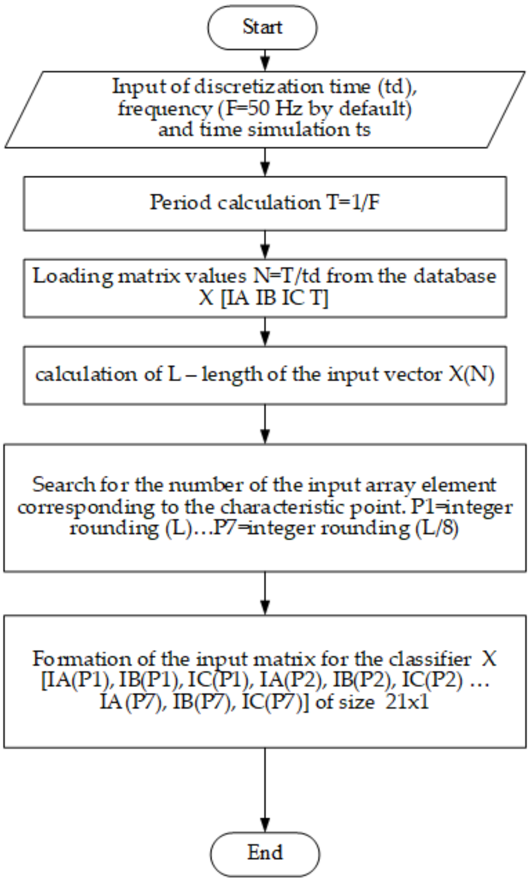


**Figure 2.** Data preprocessing algorithm.

The advantage of this algorithm is the independence from the parameter of signal reception time, because in the systems, time synchronization between the devices and the computational algorithm is a rather difficult task. The input and selection of td is determined by the technical capability of the sensors and the ADC converter. In our case this value is 0.0001 s. In addition, when applying this algorithm, it should be considered that the classification is not carried out in the motor starting moments. Therefore, the algorithm should provide for the start of operation from a time of 2–5 s, i.e., a time greater than the motor start time.

Since the purpose is to investigate the possibility of applying classification algorithms methodology, data classification in the work will be used widely for similar problems. Therefore, to achieve this objective, two of the most common methods for solving such classification problems have been chosen: the support vector machine (SVM) method [35] and K-nearest neighbors [36]. However, due to the fact that the data on motor defects are quite massive, it is necessary to develop methods to ease the mathematical or computational burden on the algorithm. Each experiment set in this paper corresponds to its own classification algorithm. In this case, in the final version these algorithms should be combined into an ensemble [37]. Figure 3 shows the algorithm for combining the developed classification algorithms into one ensemble.

The algorithm in Figure 3 is an algorithm adapted for the issues to be solved by the stacking-principle of ensembling [38]. In this algorithm, the important issue is the calculation of the probability of belonging to the class N. This parameter is determined on the basis of the neural network algorithm solving the regression problem, where the probability of membership is calculated by a regression model pre-trained on the available information [39].

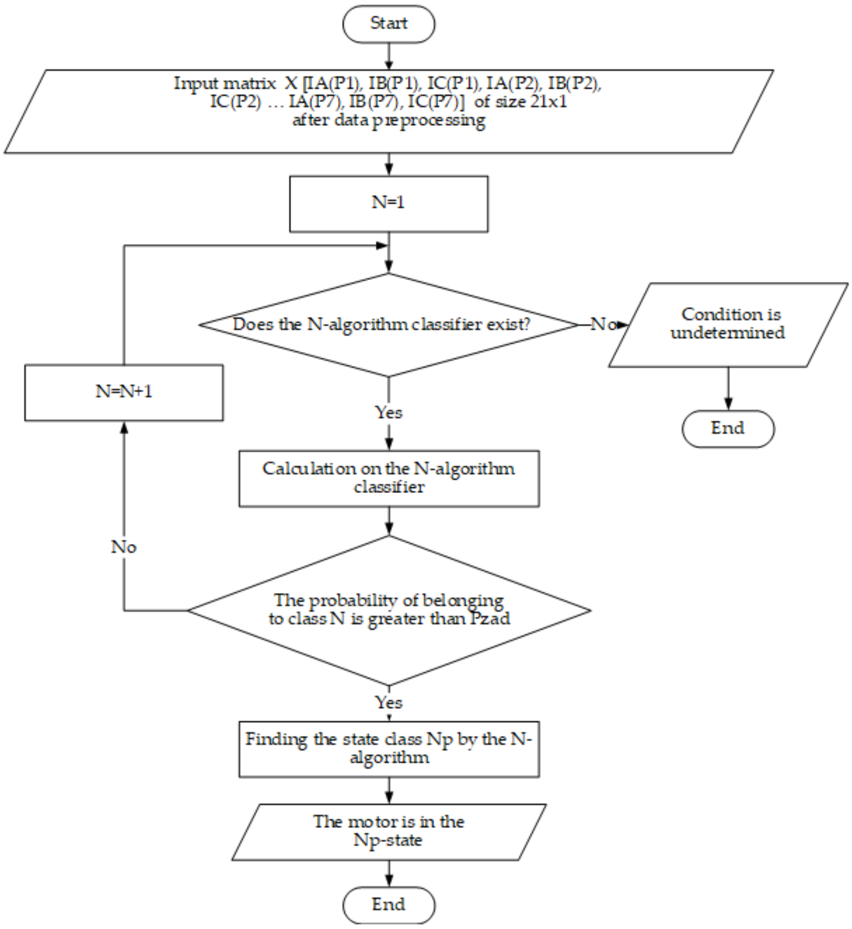


**Figure 3.** Ensemble Learning Algorithms.

## 3. Experiments

This study is a preliminary study before a series of experiments on laboratory equipment (Figure 4).

**Figure 4.** Equipment for experiments.

Laboratory equipment is a cascade of two induction motors (corresponding to the passport data): 1—test motor, 2—load motor. The latter simulates the moment of resistance of the working body (pump, fan). Regulation of the resistance moment is realized by means of an Altivar Schneider Electric ATV630U30N4 frequency converter. To collect data on the laboratory equipment, the single-board PC Raspberry Pi with a High-Precision AD/DA Board expansion board is used.

The present preliminary study is an attempt to investigate the possibility of using clustering techniques to determine motor faults. These are taken from the power flow parameters on the common power bus without considering data from the distribution networks taken directly from each machine.

The experiments in this paper have been performed only on model data. According to the simplified structure of the power supply system (Figure 1), its simulation model (Figure 5), consisting of mathematical models of an induction motor [40,41], nonlinear load [42] and filter-compensating device [43] is implemented.

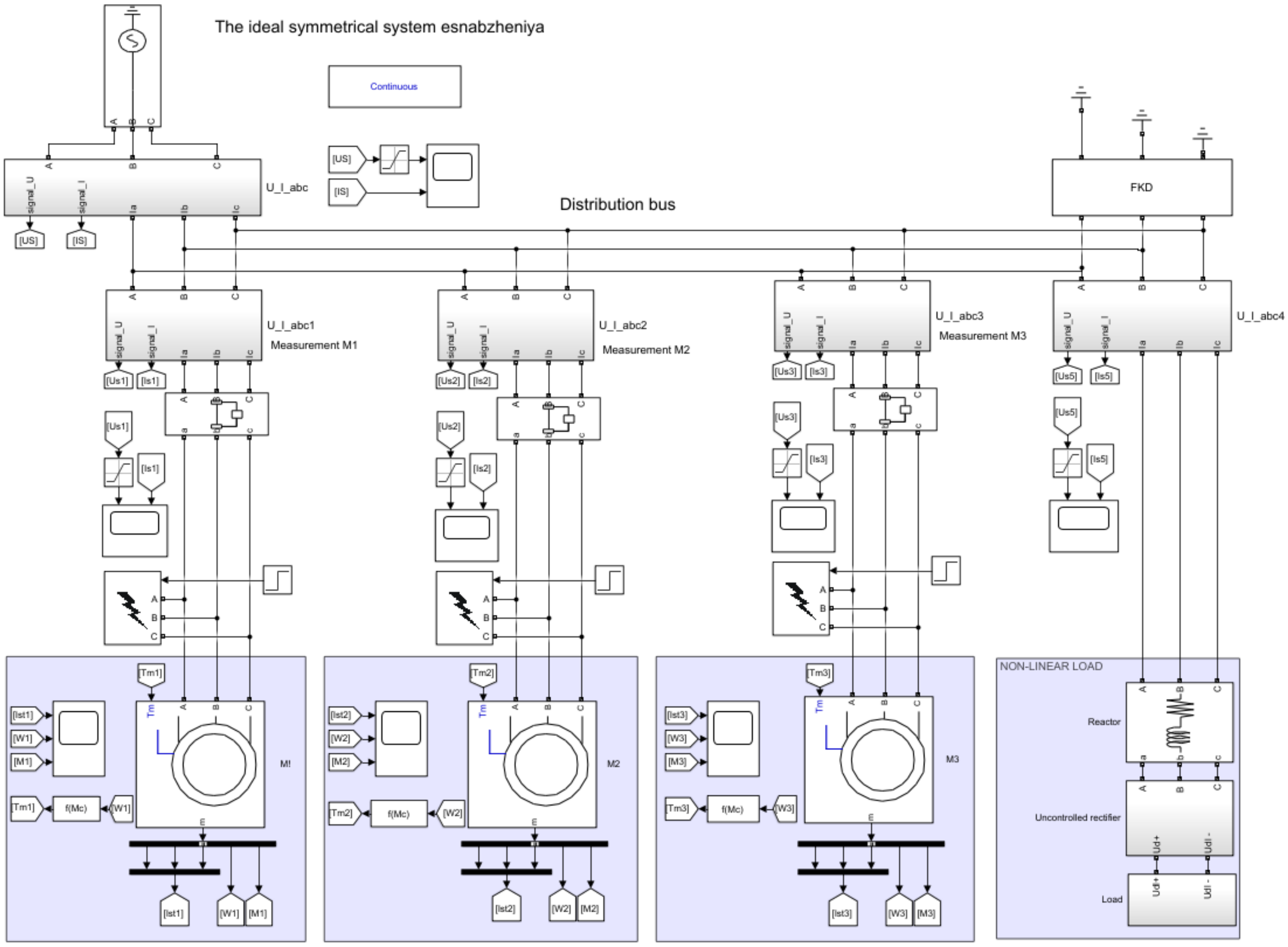


**Figure 5.** Simulation model of the power supply system for a group of induction motors.

This simulation model (Figure 5) includes models of three induction motors. Their parameters are presented in the Table 1. The model was executed in the Simulink environment.

**Table 1.** Motors parameters.

| Scheme Symbol | Name | Power $P_{nom}$, kW | Current, $I_{nom}$, A | n, r/min | Cos$\varphi$ | Efficiency Factor, % | $\lambda$ | $K_p$ | $K_i$ |
|---|---|---|---|---|---|---|---|---|---|
| M1 | АИР 71 B4 | 0.75 | 2.00 | 1360 | 0.80 | 71.3 | 2.3 | 2.2 | 5.7 |
| M2 | АИР 80 B4 | 1.50 | 3.60 | 1390 | 0.80 | 78.7 | 2.3 | 2.3 | 6.2 |
| M3 | АИР 132 M4 | 11.00 | 23.40 | 1450 | 0.82 | 87.1 | 2.3 | 2.2 | 6.8 |

$U_{nom}$ = 380 V, the motors are wired in a star configuration, $\lambda$—overload capability, $K_p$—multiplicity of starting moment; $K_i$—starting current ratio.

A series of five experiments was performed on the simulation model (Figure 5). Voltages [Us] and currents [Is] consumed from the common power supply network were recorded in all series of experiments. Additionally, voltages and three-phase currents consumed by individual motors were recorded: M1—[Us1] and [Is1], M2—[Us2] and [Is2], M3—[Us3] and [Is3]. However, these parameters for this series of experiments are redundant and were removed to obtain more information about the model and to further test its adequacy. All series of experiments were conducted according to the general algorithm shown in Figure 6.

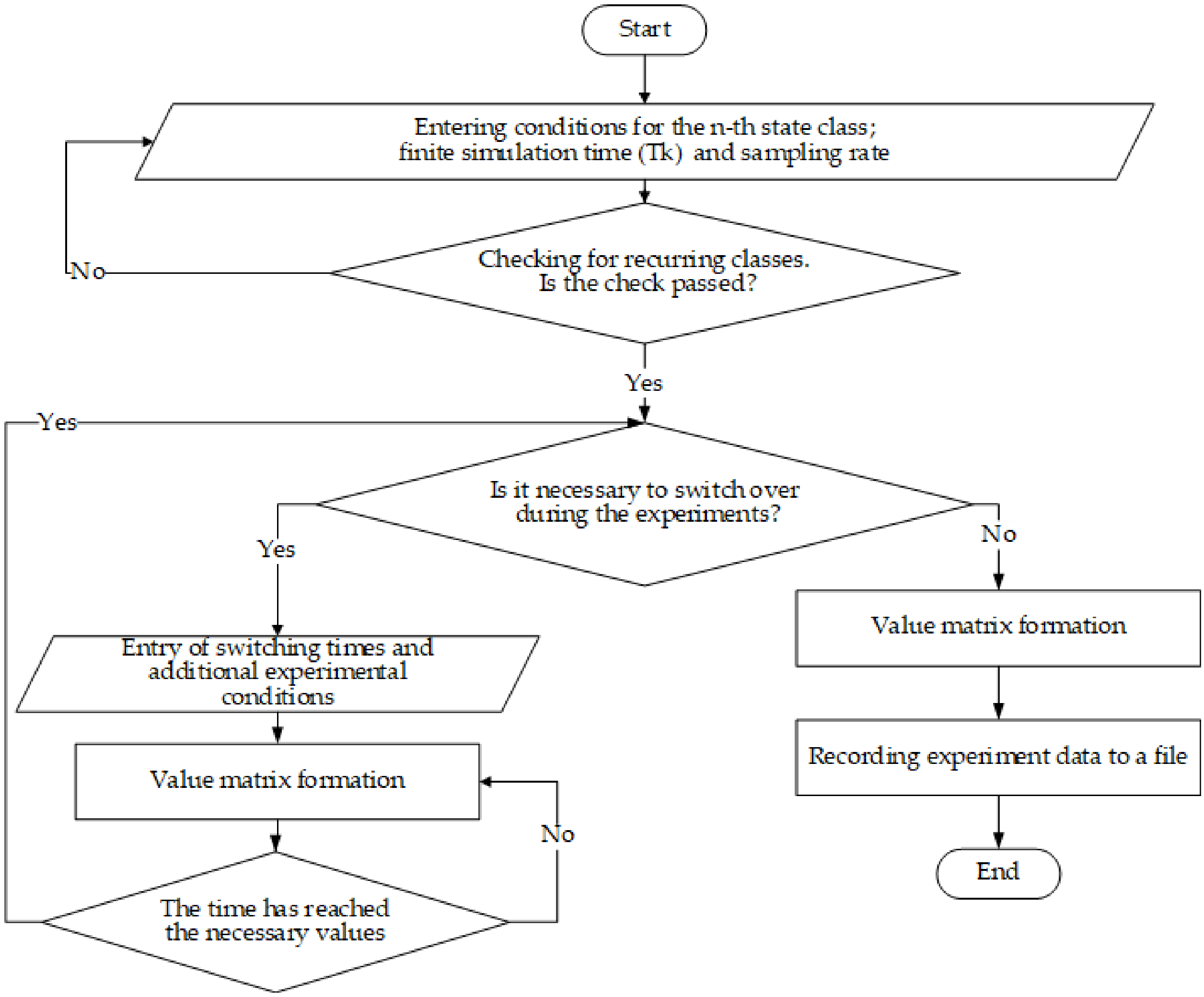


**Figure 6.** General algorithm for conducting experiments.

The sampling rate for each model experiment was chosen as 0.1 ms. At the same time, the rate on the real object could be significantly higher, because of the difficulty in capturing parameters with a rate lower than 10–100 ms on real objects [44]. The simulation time in each series of experiments was 30 s.

*3.1. Experiment 1*

Determination of the number and type of motors in operation at different motor powers. Table 2 shows the parameters of the motor substitution scheme, necessary for the experiment.

**Table 2.** Parameters of the motor substitution diagram.

| Scheme Symbol | Name | $L_s$, H | $L_r$, H | $L_m$, H | $R_s$, Ohm | $R_r$, Ohm |
|---|---|---|---|---|---|---|
| M1 | АИР 71 В4 | 1.4880 | 1.4913 | 1.4782 | 15.5812 | 8.8305 |
| M2 | АИР 80 В4 | 0.8282 | 0.8353 | 0.8071 | 7.2652 | 4.0851 |
| M3 | АИР 132 М4 | 0.1456 | 0.1475 | 0.1402 | 0.5216 | 0.3055 |

The condition for conducting the experiments is that the motors are alternately switched on in operation. During the experiments, eight sets of data are formed, corresponding to eight classes. Each class represents data with a certain motor state (a total of three motors, nine states, the state in which all motors are switched off is not considered).

### 3.2. Experiment 2

Determination of the number of motors in operation at the same power of the motors. Table 3 shows the parameters of the motor substitution scheme, necessary for the experiment.

**Table 3.** Parameters of the motor substitution diagram.

| Scheme Symbol | Name | $L_s$, H | $L_r$, H | $L_m$, H | $R_s$, Ohm | $R_r$, Ohm |
|---|---|---|---|---|---|---|
| M№1 | АИР 132 М4 | 0.1453 | 0.1473 | 0.1400 | 0.5212 | 0.3051 |
| M№2 | | 0.1455 | 0.1474 | 0.1401 | 0.5214 | 0.3053 |
| M№3 | | 0.1456 | 0.1475 | 0.1402 | 0.5216 | 0.3055 |

The conditions of the experiment correspond to Experiment 1. In this series of experiments eight data sets are formed, corresponding to eight classes.

### 3.3. Experiment 3

Determination of mode and load of induction electric motor. The experiment is carried out with fan-loaded motors of different capacities. Different combinations of load set/reset of different magnitudes relative to rating moment in % as well as its time interval. M№1—30 s set/reset at 10–20 s intervals, M№2—30 s set/reset at 14–26 s intervals, M№3—30 s set/reset at 8–24 s intervals. The experiments generate 12 data sets corresponding to twelve classes.

### 3.4. Experiment 4

Determination of the fault and its magnitude, taking into account the operation and load of the induction motor. For this purpose, when the electric motor was running, the switch was used to short the winding turns $W_{s.c.}$ to a shunt with a resistance that provided a given value of current $I_{s.c.}$ This corresponded to the occurrence of short-circuit fault of the winding turns with a given depth of short circuit:

$$K_{s.c.} = \frac{W_{s.c.} \cdot I_{s.c.}}{I_1 \cdot W_w} \cdot 100\%, \tag{8}$$

Short circuit simulation time intervals for each motor: M1—interval 30 s short circuit in 15 s, M2—interval 30 s short circuit in 22 s, M3—interval 30 s short circuit in 26 s. In this series of experiments, 24 sets of data are generated, corresponding to 24 classes.

### 3.5. Experiment 5

Determination of the fault and its magnitude, taking into account the operation and load of the induction motor, taking into account the non-linear load in the network. The experiment is conducted by simulating the fault (one single-phase fault) at different fault depths and taking into account the influence of non-linear consumers in the point of common connection. In the course of the experiments, 12 data sets are formed, corresponding to twelve classes.

## 4. Results and Discussion

### *4.1. Research of Changes in the Energy (Current) Characteristics of an Induction Electric Motor When Defects Occur*

Figure 7 shows the change in the electrical characteristics of the induction electric motor in normal operating condition without any defects.

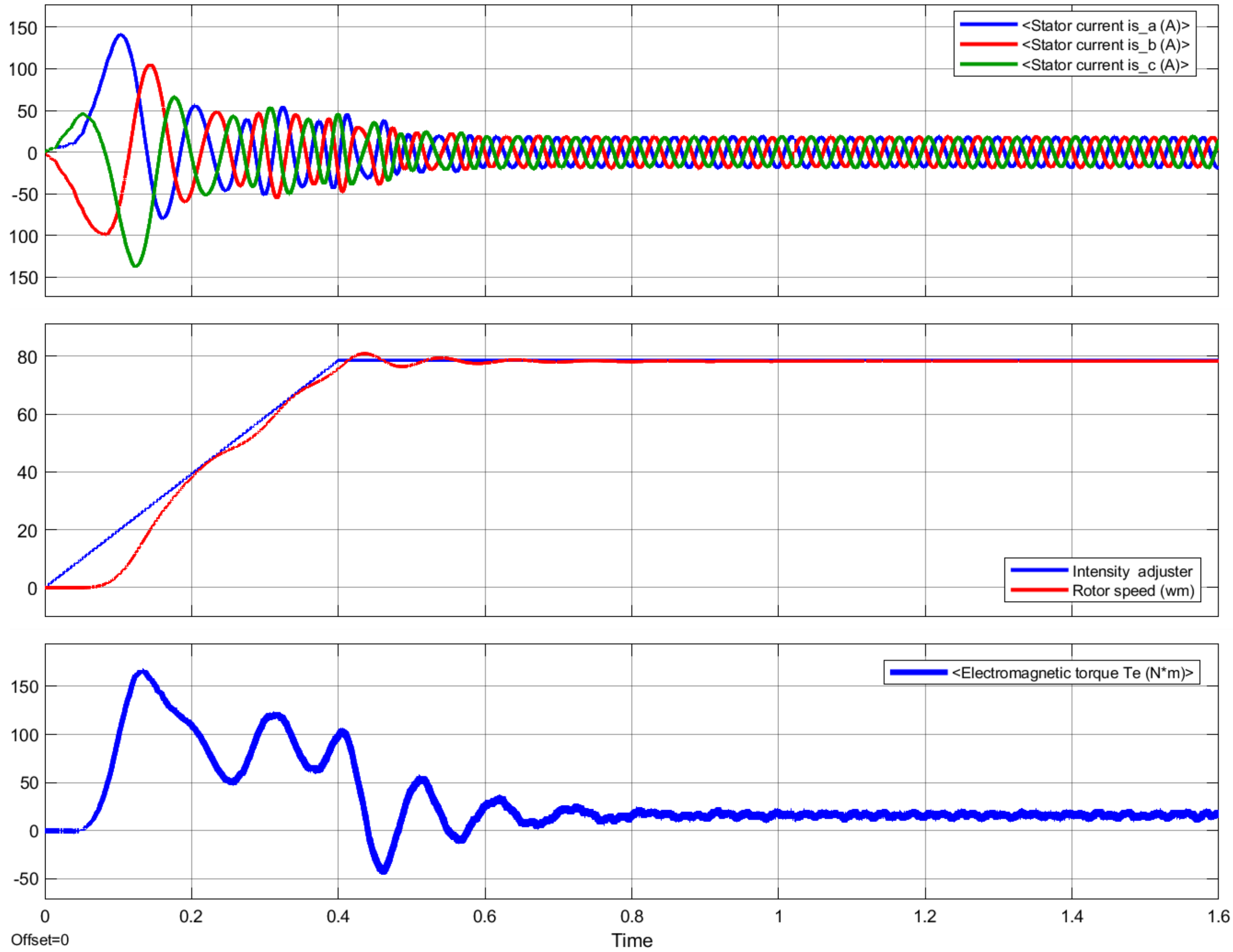


**Figure 7.** Oscillograms of electric motor output coordinates in normal operating condition without defects.

The top panel of Figure 7 shows the stator current diagrams for phase A (green), phase B (red) and phase C (yellow). The middle panel shows the rotor speed variations (red) and the output coordinate of the controller which controls the rotor speed (blue) in time. The bottom panel presents the change in electromagnetic moment in time. Figure 8 shows the change in the harmonic distortion coefficient $K_I$ and the electromagnetic moment ripple coefficient $\Sigma K_p$ in time.

As can be seen in Figures 7 and 8, the change in the character of the oscillograms occurs only in the starting moment of the motor. The amplitude of the currents begins to grow from the moment the motor starts. At the moment the stator speed reaches the steady-state value, the amplitude of stator currents decreases sharply, and smoothly reaches the steady-state value in 0.2 s. The same character of changes can be seen for the electromagnetic moment. At the moment of 1 s, it sharply decreases and gradually in 0.2 s reaches the steady-state value.

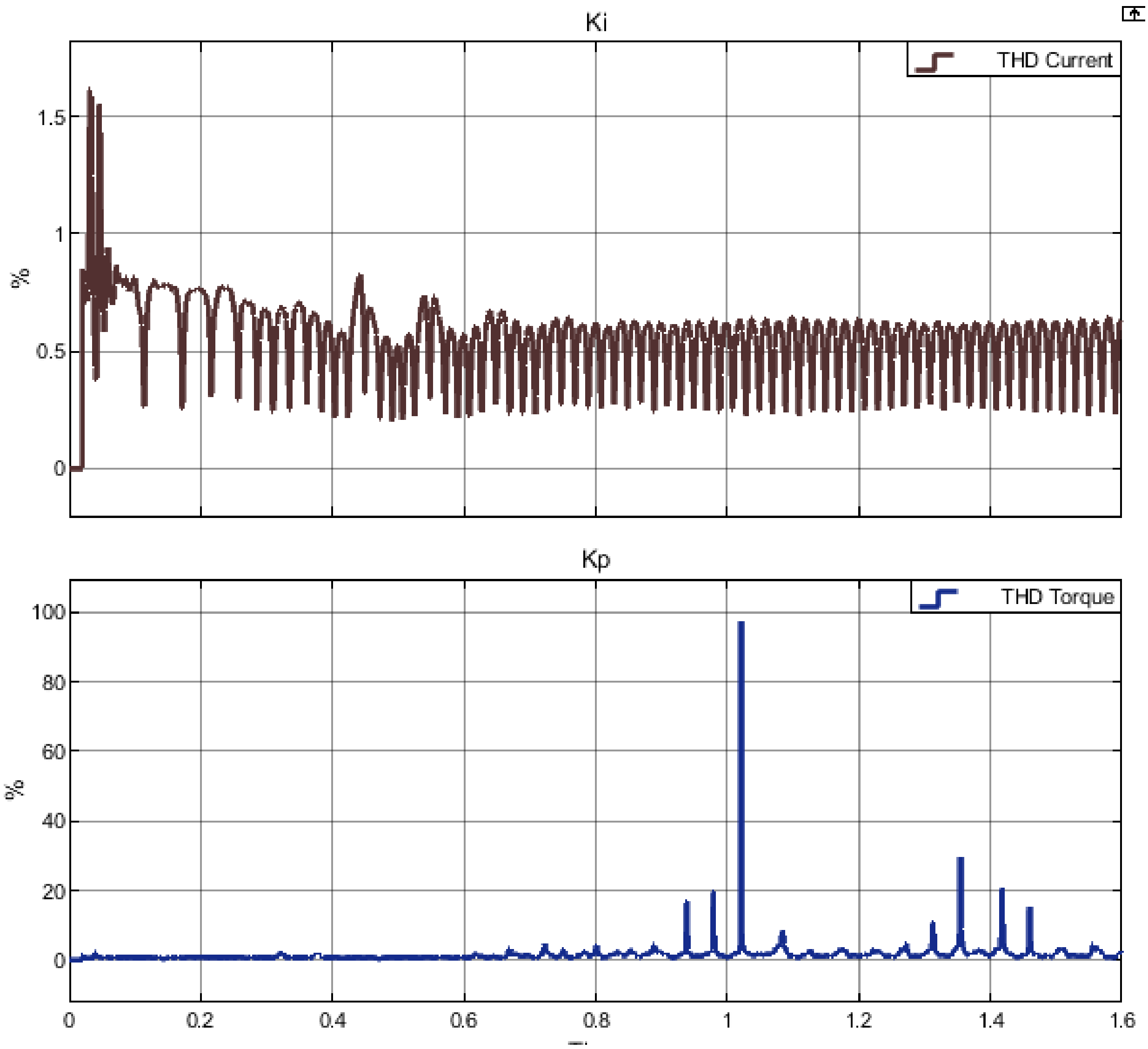


**Figure 8.** Change in harmonic distortion coefficient $K_I$ and electromagnetic moment pulsation coefficient $\Sigma K_p$ in normal operating state of electric motor without defects.

Figures 9 and 10 present the same characteristics as in Figures 7 and 8, but including simulated short-circuit in phase A-B at time t = 0.8 s in steady-state. The current oscillograms (top picture of Figure 9) show at t = 0.8 s (time of simulation of the defect) a sharp increase in the current amplitude for 0.1 s and a further change in the shape and amplitude of the current consumed by the induction motor. They also demonstrate an increase in the frequency and amplitude of the ripple. At the moment of time 0.8 s we can see a sharp increase in the harmonic distortion coefficient $K_I$ for a period of about 0.1 s and its further increase; a sharp increase in the electromagnetic moment $\Sigma K_p$ and the scatter of its amplitude after 0.1 s. The described changes in the electric characteristics of the electric motor undoubtedly show the negative impact of the occurrence of this type of defect on the motor. The defect actually reduced the energy and mechanical capabilities of the electric motor. However, the main result is the proof of the influence of the defect on the changes in the character of the current components of the electric motor. That means it is possible to solve the inverse problem—by the character of changes in current components it is possible to assess the presence of a particular defect. That is, to assess the actual state of the electric motor.

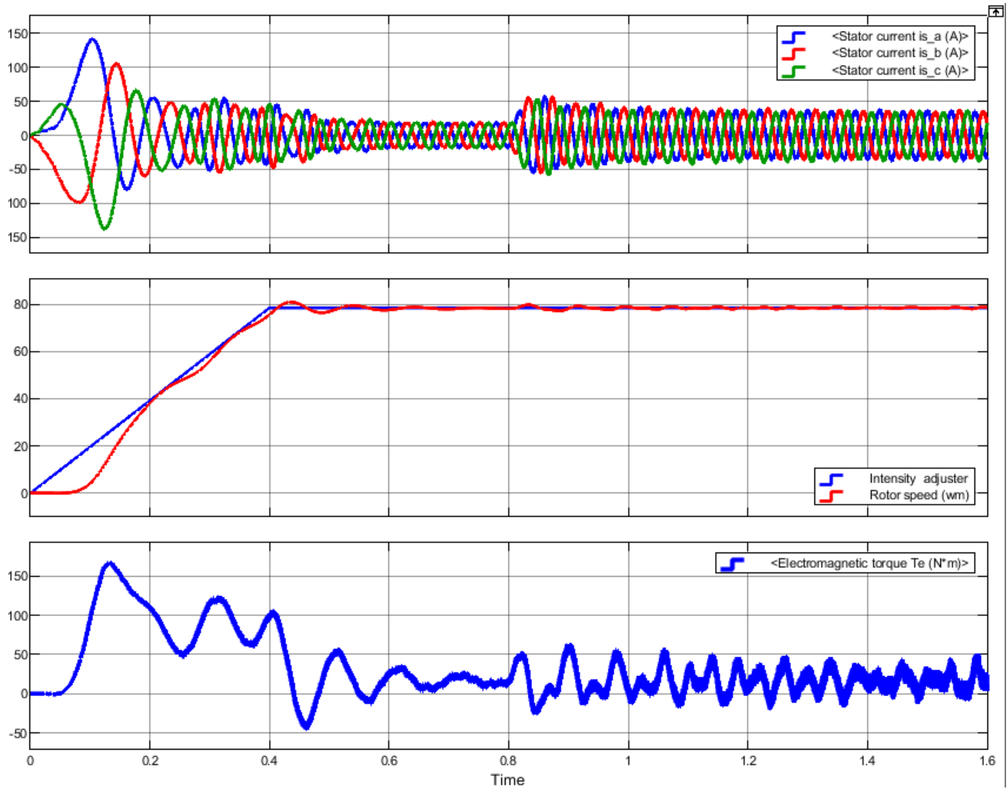


**Figure 9.** Oscillograms of output coordinates of the electric motor when simulating a short circuit in phase A–B at the time t = 0.8 s in the steady state.

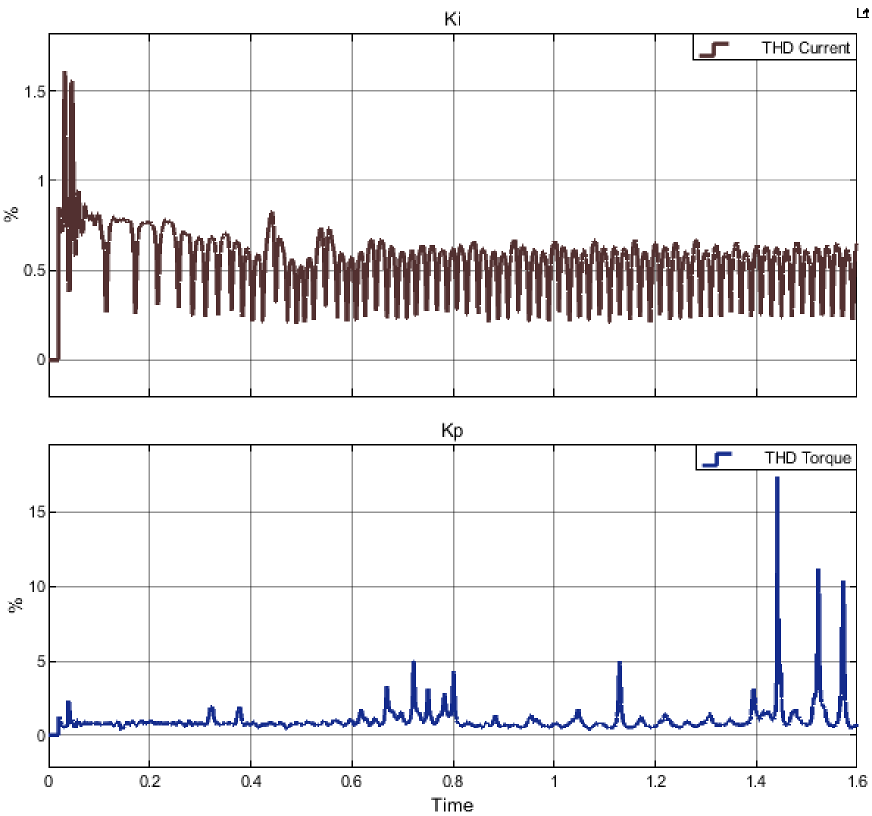


**Figure 10.** Change in harmonic distortion coefficient $K_I$ and electromagnetic moment ripple coefficient $\Sigma K_p$ during short-circuit modeling in phase A–B at the time t = 0.8 s in the steady state.

### *4.2. Simulation of a Simplified Power Supply System with Individual Motor Control and Total Energy Flow Control*

Figures 11–13 show the results of the simulation model (Figure 5).

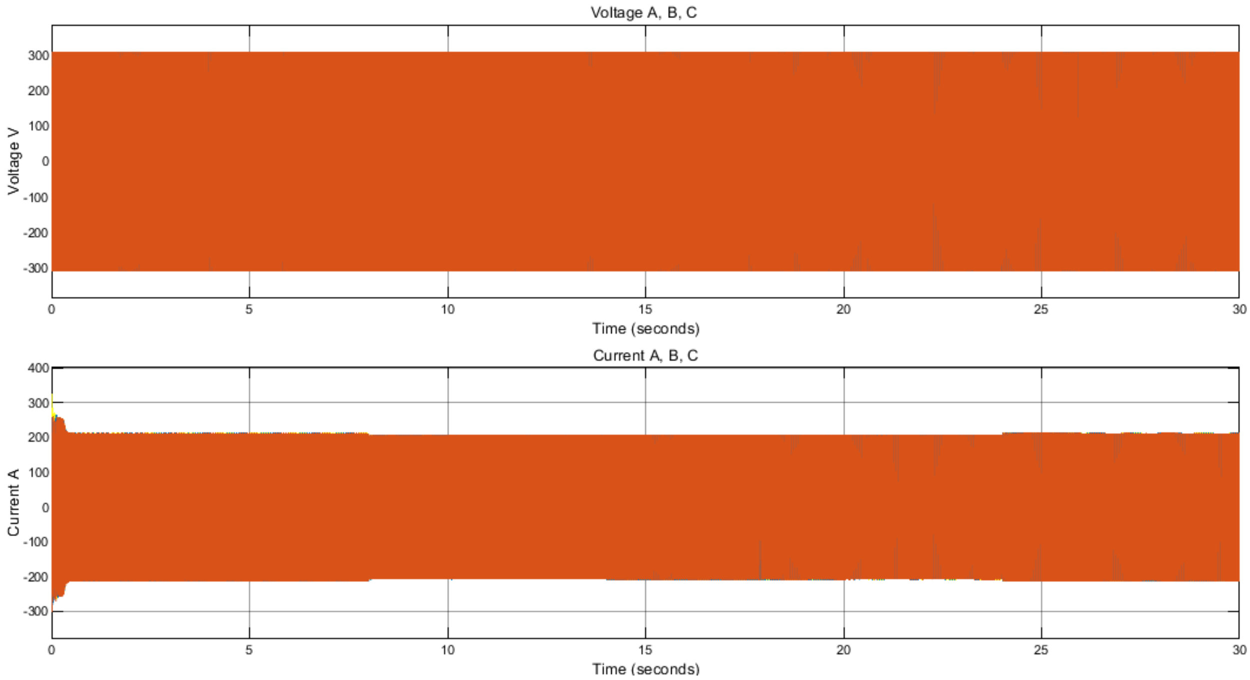


(***a***)

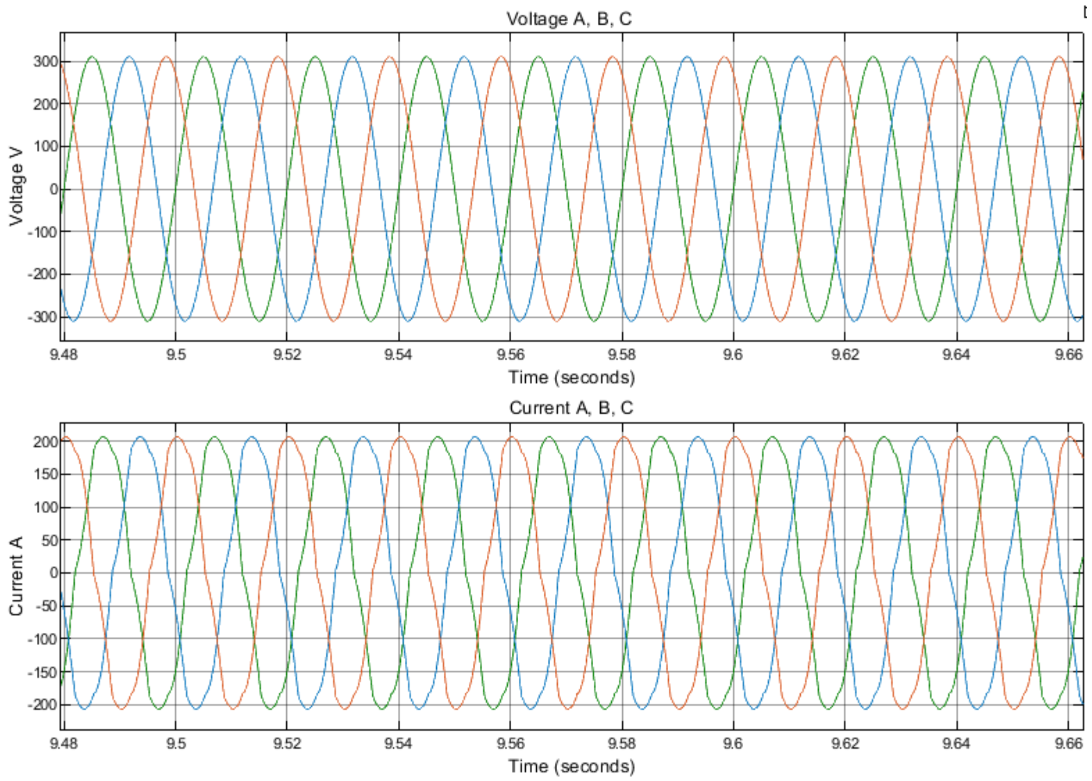


(***b***)

**Figure 11.** Results of the power supply system simulation model for a group of asynchronous motors. (***a***)—*general level of current and voltage changes on the common bus;* (***b***)—*shapes of current and voltage on the common bus*.

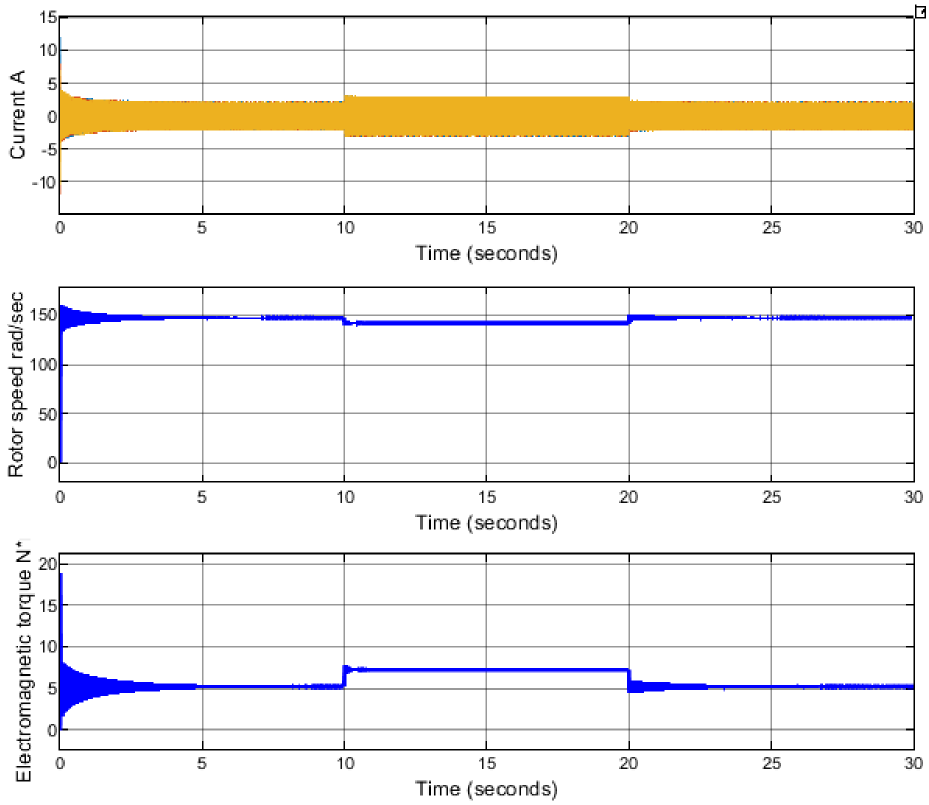


(**a**)

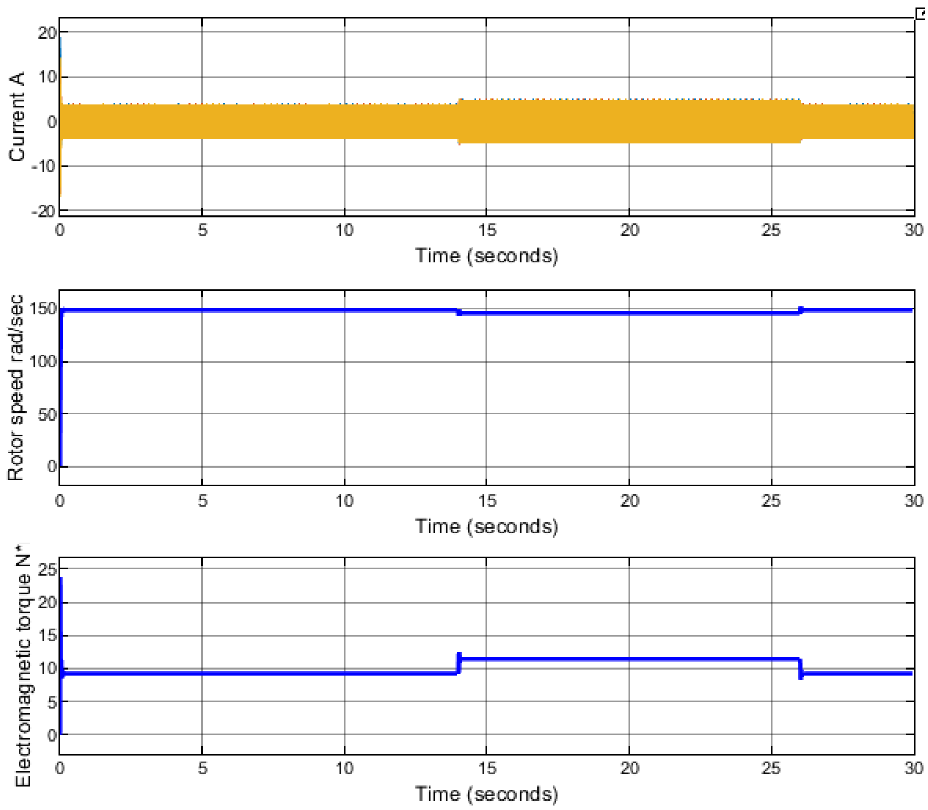


(**b**)

**Figure 12.** *Cont.*

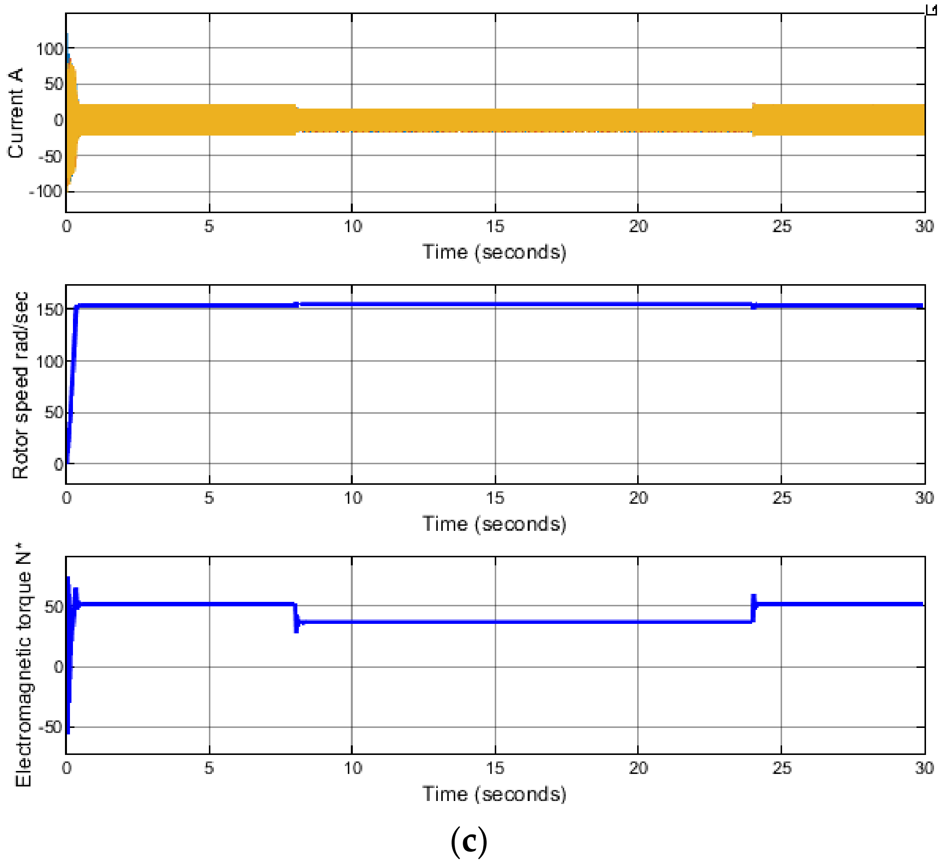


**Figure 12.** Results of the power supply system simulation model for induction motors. (***a***)—*M1: Current, rotor speed and moment measurements for Motor1*; (***b***)—*M2: Current, rotor speed and moment measurements for Motor 2*; (***c***)—*M3: Current, rotor speed and moment measurements for Motor 3*.

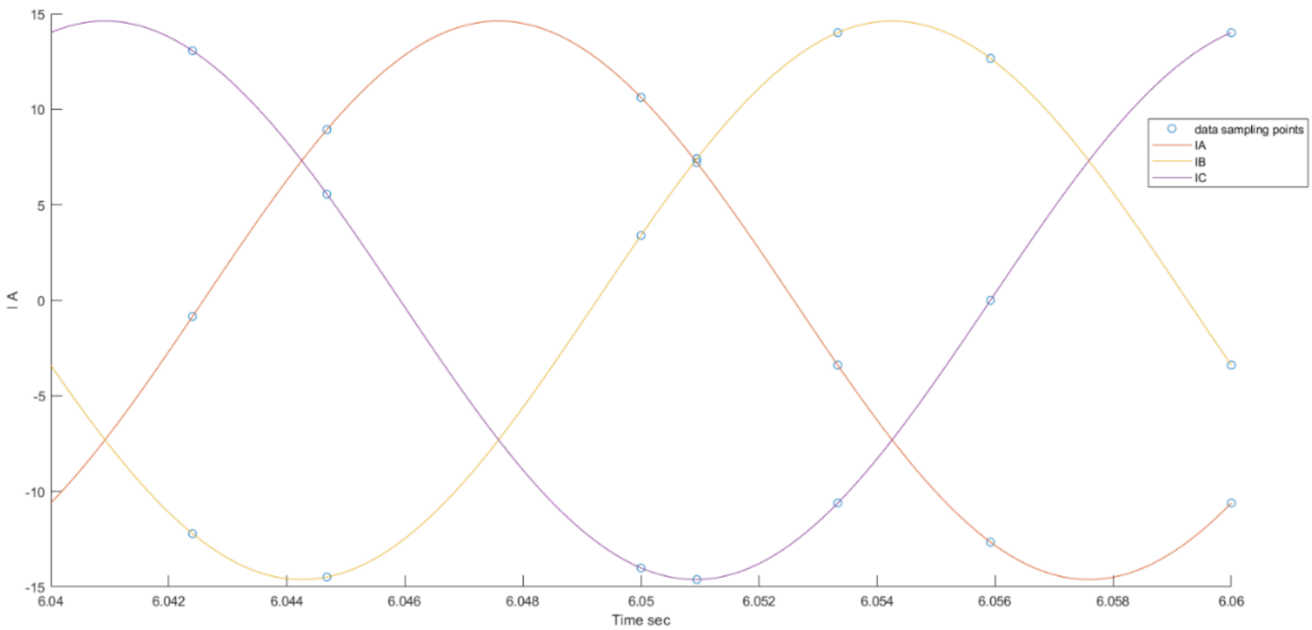


**Figure 13.** Visual representation of the data preprocessing result.

Figure 11 presents the results of the simulation model of the power supply system for a group of induction motors. The current values for each phase are measured on the common bus.

As can be seen on Figure 11, the current value changes rapidly between 0 and 1 s. That corresponds to the starting moment of the motor. In the time period of 1 s the amplitude of the current fluctuations stabilizes. In addition, zones of amplitude decrease in the time period from 8 to 24 s can be seen. This is due to changes in the load on the motors at different time intervals (Figure 12). The voltage values are stable in amplitude and frequency regardless of external factors and motor condition. Analysis of voltage values in this form is not possible, because they do not carry the necessary information. However, on a real site the voltage values are also subject to analysis due to imperfections in the electrical networks. Directly on the site changes in voltage values can be correlated with the occurrence of various defects. However, this fact requires additional research.

When motors of different powers are supplied from a common bus with changes in operating modes, load or technical condition, the current consumption of individual motors changes, but only minor deviations are possible on the common bus. Under such conditions, disturbances occurring in an individual less powerful motor have no effect on the power system (Figure 11). Changes in output coordinates (current, speed and moment) will cause significant damage.

Characteristics of model and experimental data will be used at the stage of data processing and allocation of essential features.

### *4.3. Preparing Data for Classification*

Figure 13 shows the result of preprocessing the data.

The points on the graph have been obtained by executing the algorithm shown in Figure 2. The execution of the algorithm resulted in a significant reduction of the training sample. The size of the training sample is $21 \times N_k$, where $N_k$ is the number of frames ($N_k = 30/0.02 = 1500$). To form such a sample, seven characteristic points per frame are extracted. In this case, an additional reduction up to five points is possible. However, it is not possible to fully test such an effect on model data, since they are idealized and do not pass the filtering procedure. They are not affected by random noise and disturbances. An important factor when preparing the data is the consistency of the data in the training sample and when feeding to the working classification algorithm. When developing the sample, the sequence of points from increasing to decreasing time or vice versa should be observed. The chosen principle of sequentially ascending or descending data placement should be the same at the moment of learning, testing, and using the classification algorithm. This point is essential for data processing and the application of classification algorithms. To form a data sample for the construction of a classifier model in five experiments, the simulation time of 30 s was divided into frames of 2 s each. According to the algorithm on Figure 2, seven characteristic points were selected in each frame. The array of data for training, testing and verification of the classifier was formed.

### *4.4. Data Classification*

Figure 14 shows the occurrence of the data set of experiment 1.

As can be seen in Figure 14, the data looks well classified—no overlaps, outliers, etc. Indeed, after training by SVM and KNN algorithms, the errors on the test data are 0%. However, when the data set was formed by shifting the data frame by half a period, which is 0.01 s, the accuracy of this model decreased significantly and was 70%. To solve this issue, the model was additionally retrained on half-period data. After retraining, the accuracy increased to 89%. Thus, to increase the accuracy, the training sample should be expanded to include data broken down by half-period.

Figure 15 shows the occurrence of the data set of experiment 2.

Visualization of the data set of experiment 2 showed redundant introduction of classes for the second experiment. Classes 1 and 2 completely overlapped with each other, as did classes 5 and 6. In this experiment, the number of classes can be reduced from seven to five. The results of this classifier model were similar to the results of experiment 1. In order to level this fact, an operator for checking the data for recurrent classes was added to the experiment's algorithm (Figure 3) in the future.

Figure 16 demonstrates the occurrence of the data set of experiment 3.

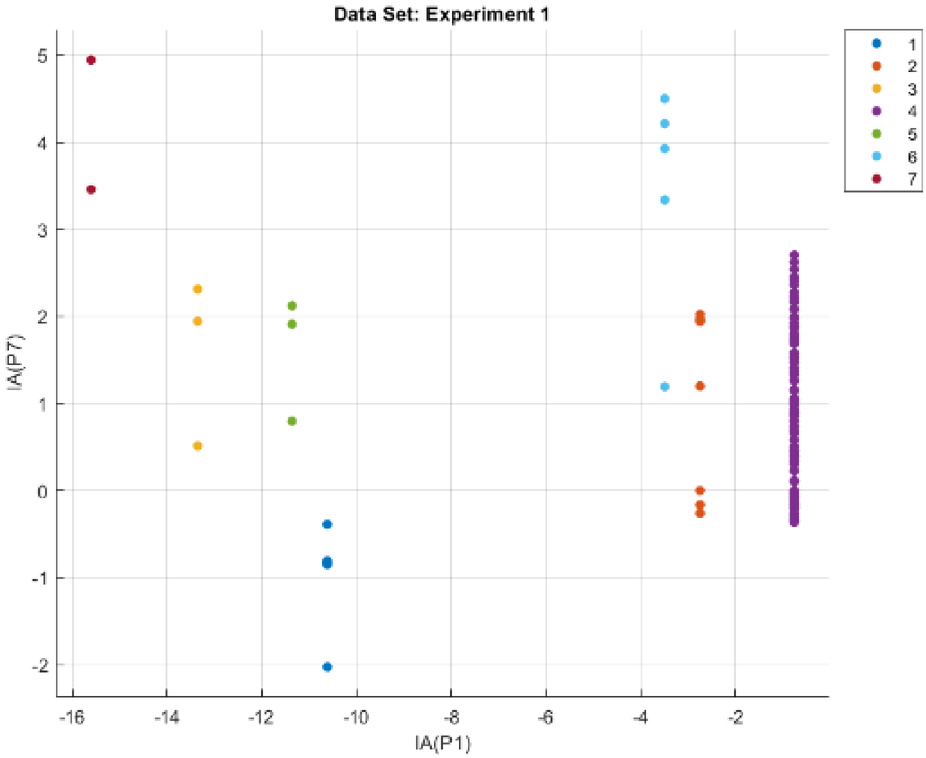


**Figure 14.** Data set of experiment 1.

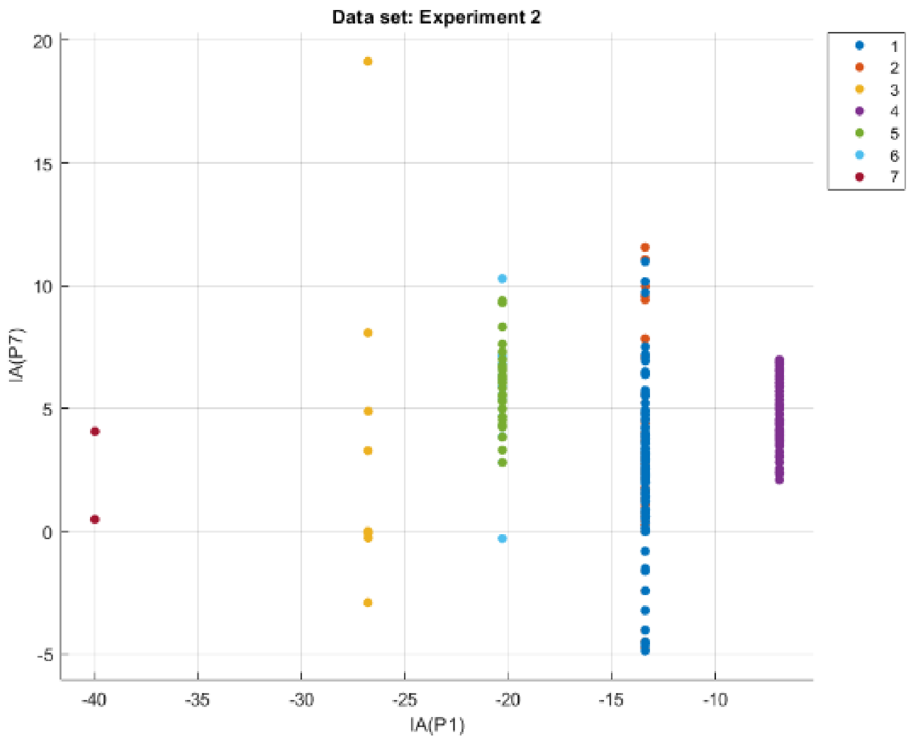


**Figure 15.** Data set of experiment 2.

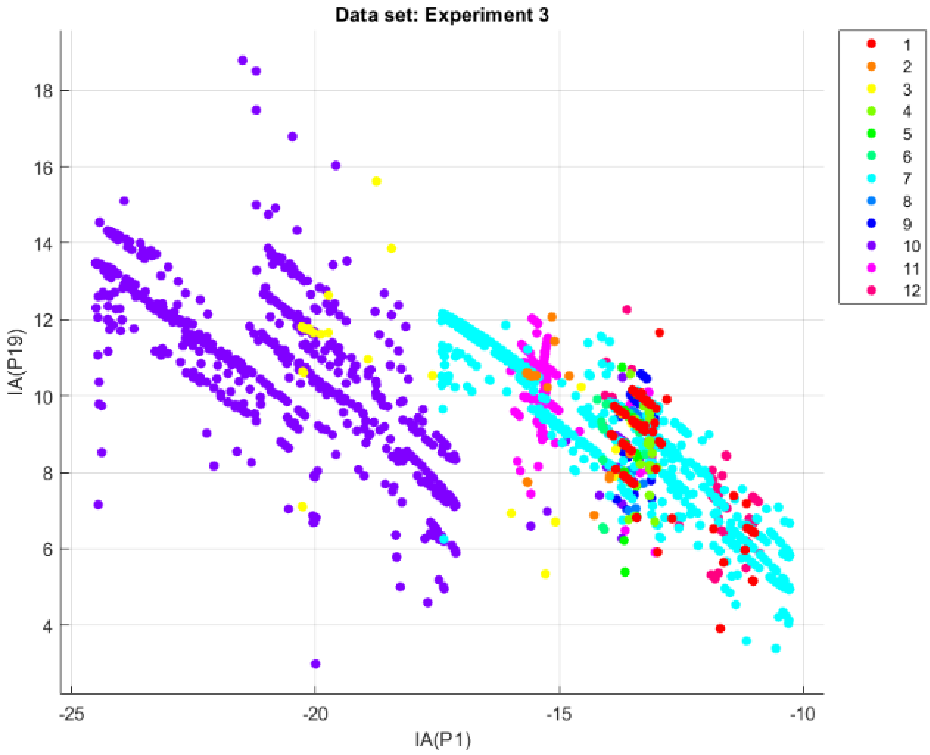


**Figure 16.** Data set of experiment 3.

Figure 17 presents the occurrence of the data set of experiment 4.

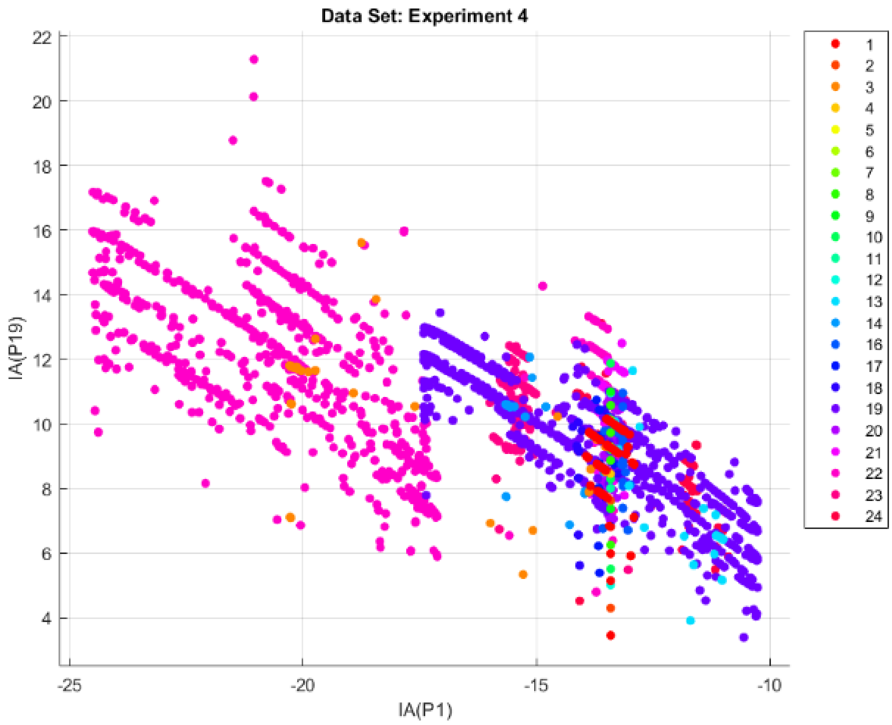


**Figure 17.** Data set of experiment 4.

Figure 18 shows the occurrence of the data set of experiment 5.

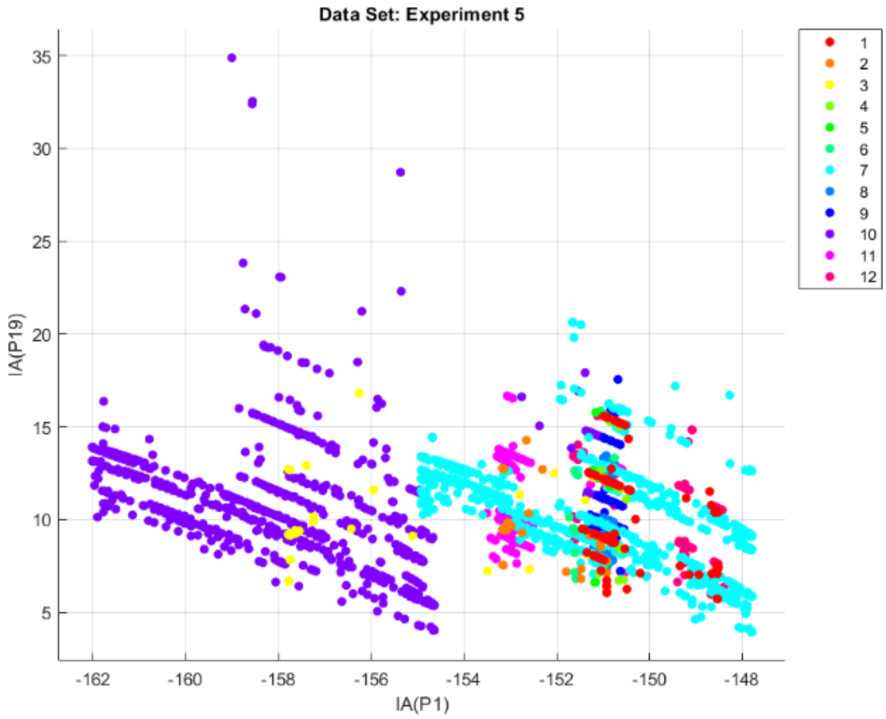


**Figure 18.** Data set of experiment 5.

Figure 19 shows the confusion matrix, obtained after the classification method SVM.

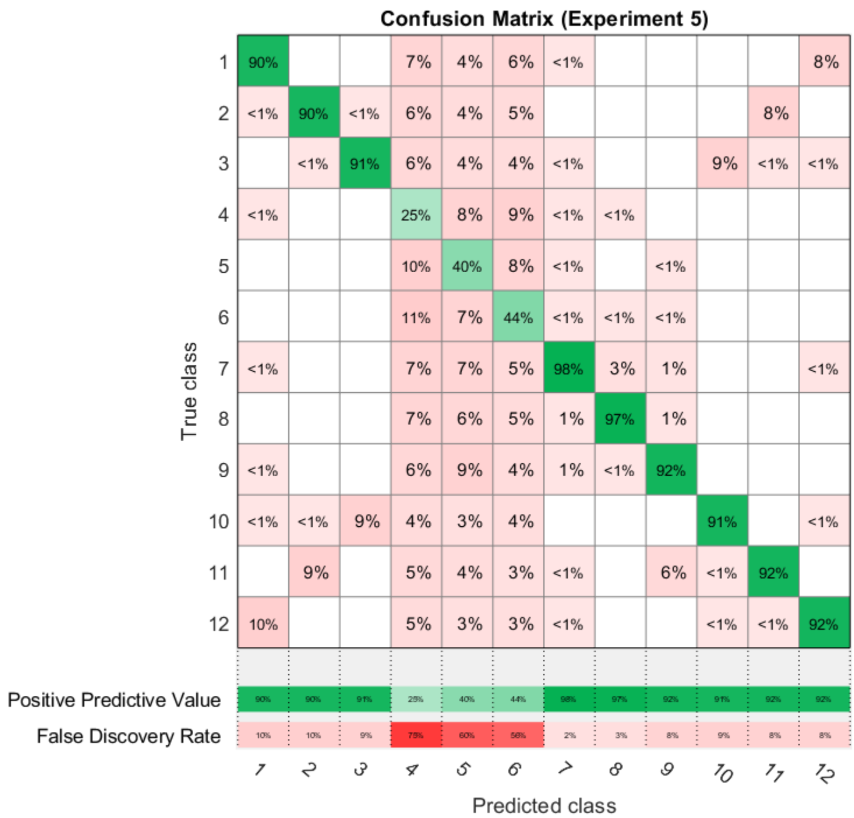


**Figure 19.** Confusion matrix. Experiment 5.

The classification process on the data sets of experiments 3, 4, and 5 was of the same nature. The model was trained using the SMA method. The accuracy obtained from the raw data for all three experiments did not exceed 67%. For instance, for experiment 5, the accuracy was only 63.7%. However, the Confusion matrix for experiment 5 shows that the major problem affecting accuracy performance is classes 4, 5, and 6. After removing these classes, the classifier trained with an accuracy of 84.7%, which significantly improved the results. At the same time, the organization of classes 4, 5, and 6 and the development of a separate classifier for them shows that the accuracy of this model is 92.1%. Thus, separating the classifiers for different datasets and then ensembling them is more preferable and easier to implement than training a classifier model on all data at once.

## 5. Conclusions

In he course of the present work, on the whole, it is possible to prove the consistency of the hypothesis. This means that the state of induction motors connected to a common power supply bus can be identified by the electrical components (current and voltage) recorded on the common section bus by classifying and recognizing a certain state of the electric motor in normal operation and when a defect occurs. In this case, it is necessary to especially highlight a number of points:

(1) in the paper, only the values of the current strength are considered as the energy parameters. Voltage is not considered because it is reference. Indeed, on real objects, voltage changes can give additional information about the object state. Therefore, under the conditions of the subsequent verification of this algorithm on a real object, it is advisable to additionally consider and evaluate the possibility of using voltage values when solving classification problems

(2) classification algorithms are meaningless without proper preparation of the datasets. In the present work, an array of points with values calculated by data preprocessing algorithms is proposed as such a set. On the model data, such an assumption showed a good result. However, on a real object, especially considering the practice of loss of sinusoidality upon the onset of defects, this method may significantly distort the picture of signs. Thus, this algorithm can be used for a rough estimate, while the data preprocessing algorithm can be extended, for example, by an additional check for the loss of sinusoidality, etc.

(3) the methodology of developing classification algorithms for the task of identifying the technical condition of induction motors groups according to the total energy flow gives the best results with the following approach: a classification algorithm for each type or class of motor condition is developed, which is then combined into an ensemble. The best way of ensembling is to calculate the probability of the model falling into a certain state class on the basis of a trained regression model

(4) The designed model can be used as an algorithm for producing a synthetic dataset, which is swept into the main dataset. Firstly, this helps to make the data sample balanced, especially in terms of the simulation of short circuits and other defects. Secondly, this allows the features of one or another class to be underlined more clearly.

(5) the results presented in this article have a noticeable theoretical character, as they are based on the reference data obtained during modeling. The paper is considered to be continued, where the developed methodology and principles of induction electric motors state identification should be tested experimentally on real equipment and in the conditions of real operating productions.

**Author Contributions:** Conceptualization, N.I.K., N.A.K. and Y.L.Z.; methodology, N.A.K. and N.I.K.; software, N.I.K.; validation, N.A.K., N.I.K. and Y.L.Z.; formal analysis, N.I.K. and N.A.K.; resources, N.I.K. and N.A.K.; data curation, N.A.K.; writing—original draft preparation, N.I.K. and N.A.K.; writing—review and editing, Y.L.Z.; visualization, N.A.K.; supervision, Y.L.Z.; project administration, Y.L.Z. All authors have read and agreed to the published version of the manuscript.

**Funding:** This research received no external funding.

**Institutional Review Board Statement:** Not applicable.

**Informed Consent Statement:** Not applicable.

**Conflicts of Interest:** The authors declare no conflict of interest.

## References


1. Malov, D.; Edemskii, A.; Saveliev, A. Architecture of proactive localization service for cyber-physical system's users. In *International Conference on Interactive Collaborative Robotics*; Springer: Cham, Switzerland, 2019; Volume 11659, pp. 10–18. [CrossRef]
2. O'Leary, P.; Harker, M.; Ritt, R.; Habacher, M.; Landl, K.; Brandner, M. Mining sensor data in larger physical systems. *IFAC-Pap.* **2016**, *49*, 37–42. [CrossRef]
3. Klyuev, R.; Fomenko, O.; Gavrina, O.; Turluev, R.; Marzoev, S. Energy indicators of drilling machines and excavators in mountain territories. In *Energy Management of Municipal Transportation Facilities and Transport*; Springer: Cham, Switzerland, 2019; Volume 1258, pp. 272–281. [CrossRef]
4. Safina, E.; Khokhlov, S. Paradox of alternative energy consumption: Lean or profligacy? *Int. J. Qual. Res.* **2017**, *11*, 903–916. [CrossRef]
5. Dobush, V.S.; Belsky, A.A.; Skamyin, A.N. Electrical Complex for Autonomous Power Supply of Oil Leakage Detection Systems in Pipelines. *J. Phys. Conf. Ser.* **2020**, *1441*, 157105. [CrossRef]
6. Ivkina, O.P.; Ziyakaev, G.R.; Pashkov, E.N. Mathematic study of the rotor motion with a pendulum selfbalancing device. *J. Phys. Conf. Ser.* **2016**, *744*, 012157. [CrossRef]
7. Salomon, C.P.; Ferreira, C.; Sant'Ana, W.C.; Lambert-Torres, G.; Borges da Silva, L.E.; Bonaldi, E.L.; de Oliveira, L.E.D.L.; Torres, B.S. A study of fault diagnosis based on electrical signature analysis for synchronous generators predictive maintenance in bulk electric systems. *Energies* **2019**, *12*, 1506. [CrossRef]
8. Lavrenko, S.A.; Shishljannikov, D.I. Performance evaluation of heading-and-winning machines in the conditions of potash mines. *Appl. Sci.* **2021**, *11*, 3444. [CrossRef]
9. Belova, M.; Iakovleva, E.; Popov, A. Mining and Environmental Monitoring at Open-Pit Mineral Deposits. *J. Ecol. Eng.* **2019**, *20*, 172–178. [CrossRef]
10. Kudelina, K.; Asad, B.; Vaimann, T.; Rassõlkin, A.; Kallaste, A. Effect of bearing faults on vibration spectrum of BLDC motor. In Proceedings of the 2020 IEEE Open Conference of Electrical, Electronic and Information Sciences (eStream), Vilnius, Lithuania, 30 April 2020. [CrossRef]
11. Malyshkov, G.B.; Sinkov, L.S.; Nikolaichuk, L.A. Analysis of economic evaluation methods of environmental damage at calculation of production efficiency in mining industry. *Int. J. App. Eng. Res* **2017**, *12*, 2551–2554.
12. Asad, B.; Vaimann, T.; Belahcen, A.; Kallaste, A.; Rassolkin, A. Rotor fault diagnostic of inverter fed induction motor using frequency analysis. In Proceedings of the 2019 IEEE 12th International Symposium on Diagnostics for Electrical Machines, Power Electronics and Drives (SDEMPED), Toulouse, France, 27–30 August 2019. [CrossRef]
13. Vasilyev, B.Y.; Shpenst, V.A.; Kalashnikov, O.V.; Ulyanov, G.N. Providing energy decoupling of electric drive and electric grids for industrial electrical installations. *J. Min. Inst.* **2018**, *229*, 41–49. [CrossRef]
14. Ivanova, T.S.; Malarev, V.I.; Kopteva, A.V.; Koptev, V.Y. Development of a power transformer residual life diagnostic system based on fuzzy logic methods. *J. Phys. Conf. Ser.* **2019**, *1353*, 012099. [CrossRef]
15. Wang, J.; Ma, Y.; Zhang, L.; Gao, R.X.; Wu, D. Deep learning for smart manufacturing: Methods and applications. *J. Manuf. Syst.* **2018**, *48*, 144–156. [CrossRef]
16. Janssens, O.; Slavkovikj, V.; Vervisch, B.; Stockman, K.; Loccufier, M.; Verstockt, S.; Van de Walle, R.; Van Hoecke, S. Convolutional neural network based fault detection for rotating machinery. *J. Sound Vib.* **2016**, *377*, 331–345. [CrossRef]
17. Jing, L.; Zhao, M.; Li, P.; Xu, X. A convolutional neural network based feature learning and fault diagnosis method for the condition monitoring of gearbox. *Measurement* **2017**, *111*, 1–10. [CrossRef]
18. Han, T.; Liu, C.; Yang, W.; Jiang, D. A novel adversarial learning framework in deep convolutional neural network for intelligent diagnosis of mechanical faults. *Knowl. -Based Syst.* **2019**, *165*, 474–487. [CrossRef]
19. Szymahski, Z.; Paraszczak, J. Application of artificial intelligence methods in diagnostics of mining machinery. *IFAC Proc. Vol.* **2007**, *40*, 403–408. [CrossRef]
20. Janjanam, D.; Ganesh, B.; Manjunatha, L. Design of an expert system architecture: An overview. *J. Phys. Conf. Ser.* **2021**, *1767*, 012036. [CrossRef]
21. Rivera, C.A.; Poza, J.; Ugalde, G.; Almandoz, G. Industrial Design of Electric Machines Supported with Knowledge-Based Engineering Systems. *Appl. Sci.* **2021**, *11*, 294. [CrossRef]
22. Rizzoni, G.; Onori, S.; Rubagotti, M. Diagnosis and prognosis of automotive systems: Motivations, history and some results. *IFAC Proc. Vol.* **2009**, *42*, 191–202. [CrossRef]
23. Barbieri, G.; Sanchez-Londoño, D.; Cattaneo, L.; Fumagalli, L.; Romero, D. A Case Study for Problem-based Learning Education in Fault Diagnosis Assessment. *IFAC-Pap.* **2020**, *53*, 107–112. [CrossRef]
24. Hernandez, J.D.; Cespedes, E.S.; Gutierrez, D.A.; Sanchez-Londoño, D.; Barbieri, G.; Abolghasem, S.; Romero, D.; Fumagalli, L. Human-Computer-Machine Interaction for the Supervision of Flexible Manufacturing Systems: A Case Study. *IFAC-Pap.* **2020**, *53*, 10550–10555. [CrossRef]
25. Wu, F.; Wang, T.; Lee, J. An online adaptive condition-based maintenance method for mechanical systems. *Mech. Syst. Signal Process.* **2010**, *24*, 2985–2995. [CrossRef]
26. Chao, M.A.; Kulkarni, C.; Goebel, K.; Fink, O. Hybrid deep fault detection and isolation: Combining deep neural networks and system performance models. *arXiv* **2019**, arXiv:1908.01529.

27. Velandia-Cardenas, C.; Vidal, Y.; Pozo, F. Wind Turbine Fault Detection Using Highly Imbalanced Real SCADA Data. *Energies* **2021**, *14*, 1728. [CrossRef]
28. Thomson, W.T.; Fenger, M. Current signature analysis to detect induction motor faults. *IEEE Ind. Appl. Mag.* **2001**, *7*, 26–34. [CrossRef]
29. Baranov, G.D.; Matus, K.I.; Vaganov, M.A.; Bubnov, E.A. Spectral analysis algorithm for the diagnosis of electrical machines. *2019 IEEE Conference of Russian Young Researchers in Electrical and Electronic Engineering. ElConRus* **2019**, *8657020*, 424–429. [CrossRef]
30. Drif, M.; Cardoso, A.J.M. Airgap-eccentricity fault diagnosis, in three-phase induction motors, by the complex apparent power signature analysis. *IEEE Trans. Ind. Electron.* **2008**, *55*, 1404–1410. [CrossRef]
31. Drif, M.; Cardoso, A.J.M. The use of the instantaneous-reactive-power signature analysis for rotor-cage-fault diagnostics in three-phase induction motors. *IEEE Trans. Ind. Electron.* **2009**, *56*, 4606–4614. [CrossRef]
32. Kotsiantis, S.B.; Kanellopoulos, D.; Pintelas, P.E. Data Preprocessing for Supervised Leaning. *Int. J. Comput. Sci.* **2007**, *1*, 111–117. [CrossRef]
33. Xiao, X.; Xiao, Y.; Zhang, Y.; Qiu, J.; Zhang, J.; Yildirim, T. A fusion data preprocessing method and its application in complex industrial power consumption prediction. *Mechatronics* **2021**, *77*, 102520. [CrossRef]
34. Li, T.H.; Song, K. Estimation of the frequency of sinusoidal signals in laplace noise. In Proceedings of the 2007 IEEE International Symposium on Information Theory, Nice, France, 24–29 June 2007; pp. 1786–1790. [CrossRef]
35. Cristianini, N.; Shawe-Taylor, J. Background Mathematics. In *An Introduction to Support Vector Machines and Other Kernel-Based Learning Methods*; Cambridge University Press: Cambridge, UK, 2000; pp. 165–172. [CrossRef]
36. Ali, N.; Neagu, D.; Trundle, P. Evaluation of k-nearest neighbour classifier performance for heterogeneous data sets. *SN Appl. Sci.* **2019**, *1*, 1559. [CrossRef]
37. Ren, Y.; Zhang, L.; Suganthan, P.N. Ensemble Classification and Regression-Recent Developments, Applications and Future Directions. *IEEE Comput. Intell. Mag.* **2016**, *11*, 41–53. [CrossRef]
38. Shklyarskiy, Y.; Skamyin, A.; Vladimirov, I.; Gazizov, F. Distortion load identification based on the application of compensating devices. *Energies* **2020**, *13*, 1430. [CrossRef]
39. Belsky, A.A.; Dobush, V.S.; Haikal, S.F. Operation of a Single-phase Autonomous Inverter as a Part of a Low-power Wind Complex. *J. Min. Inst.* **2019**, *239*, 564–569. [CrossRef]
40. Ikeda, M.; Hiyama, T. Simulation studies of the transients of squirrel-cage induction motors. *IEEE Trans. Energy Convers.* **2007**, *22*, 233–239. [CrossRef]
41. Siddiqui, K.M.; Sahay, K.; Giri, V.K. Simulation and transient analysis of PWM inverter fed squirrel cage induction motor drives. *J. Electr. Eng.* **2014**, *7*, 9–19. [CrossRef]
42. Soheili, A.; Sadeh, J.; Bakhshi, R. Modified FFT based high impedance fault detection technique considering distribution non-linear loads: Simulation and experimental data analysis. *Int. J. Electr. Power Energy Syst.* **2018**, *94*, 124–140. [CrossRef]
43. Sychev, Y.A.; Zimin, R.Y. Improving the quality of electricity in the power supply systems of the mineral resource complex with hybrid filter-compensating devices. *J. Min. Inst.* **2021**, *247*, 132–140. [CrossRef]
44. Jung, J.H.; Lee, J.J.; Kwon, B.H. Online diagnosis of induction motors using MCSA. *IEEE Trans. Ind. Electron.* **2006**, *53*, 1842–1852. [CrossRef]